

FreshSpec: Sashimi Freshness Monitoring with Low-cost Multispectral Devices

Yinan Zhu*, Haiyan Hu*, Baichen Yang, Qianyi Huang, *Member, IEEE*, Qian Zhang†, *Fellow, IEEE*, Wei Li†

Abstract—Monitoring sashimi freshness, *i.e.*, histamine levels, in showcases poses a critical challenge for sushi restaurants and fresh food stores. Current histamine monitoring methods involve labor-intensive chemical experiments or expensive devices, making affordable on-site monitoring difficult. This paper proposes FreshSpec, a low-cost and automatic spectral imaging system capable of precisely monitoring histamine levels in sashimi with minimal human intervention. The low concentration of histamine, combined with the potential for other ingredients to mask its spectral characteristics, complicates precise histamine level predictions using coarse or redundant spectral data from low-cost devices. To address this issue, FreshSpec employs an innovative feature-wise spectral reconstruction (SR) framework that effectively eliminates irrelevant and redundant data while preserving critical histamine-related spectral features. Specifically, we redefine the SR reconstruction target by utilizing features derived from the encoder of the spectral foundation model that is enhanced to focus on histamine-related spectral features. Furthermore, inspired by the monotonic accumulation properties of histamine over time, we propose a histamine regression model with unsupervised continual adaptation to new sashimi samples during practical deployment. Experimental results from 240 samples of salmon, tuna, and snapper demonstrate that FreshSpec achieves an R2 of 0.9319 and an RMSE of 3.101 mg/100g, comparable to laboratory spectral imaging systems, while outperforming baseline schemes with a 46.95% RMSE reduction and a 0.1631 R2 improvement.

Index Terms—Meat Freshness, Spectral Large Model, Feature-wise Spectral Reconstruction

I. INTRODUCTION

SASHIMI is popular worldwide, but there are always concerns about its freshness and safety. Data show that histamine poisoning constitutes 37% of seafood-related illnesses reported to the Centers for Disease Control and Prevention (CDC) [1]. The toxic ingredient, histamine, can rapidly increase to a lethal level in a few hours if not handled or stored properly [2], [3]. However, among the entire food supply chain, the end of the nodes such as sushi restaurants or fresh food stores are particularly vulnerable to compromising the

* Yinan Zhu and Haiyan Hu are the co-first authors. †Qian Zhang and Wei Li are the co-corresponding authors.

Yinan Zhu, Haiyan Hu, Baichen Yang, and Qian Zhang are with the Department of Computer Science and Engineering, Hong Kong University of Science and Technology, Hong Kong (e-mail: yzhuhd@cse.ust.hk; hhuap@connect.ust.hk; byangak@cse.ust.hk; qianzh@cse.ust.hk).

Qianyi Huang is with the School of Computer Science and Engineering, Sun Yat-sen University, Guangzhou 510006, China (e-mail: huangqy89@mail.sysu.edu.cn).

Wei Li is with Wuhan Union Hospital, Wuhan 430022, Hubei, China (e-mail: lsnlw@sina.com).

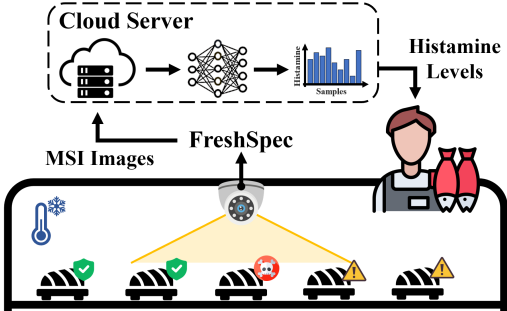


Fig. 1. Illustration of FreshSpec’s working scenario.

freshness and safety of sashimi due to fluctuating showcase temperatures [4]–[6]. As shown in Figure 1, sashimi samples can exhibit varying histamine levels simultaneously due to differences in handling and temperature. Therefore, merchants seek to monitor the histamine levels of the samples to obey the regulation and protect profits. For example, sashimi samples with histamine levels exceeding local regulations must be discarded, while those with safe but relatively high histamine levels should be sold first.

Since histamine is colorless and odorless, and even hazardous histamine levels are pretty low, *e.g.*, 5 mg/100g for U.S. Food and Drug Administration (FDA) safety level [7], existing histamine testing methods often involve high costs and complex procedures, which pose challenges for small sushi restaurants and fresh food stores. Most works require high-cost devices such as laboratory high-performance liquid chromatography [8], [9] or hyperspectral imaging (HSI) cameras [10], [11] to detect histamine, which are unaffordable for average users. Low-cost solutions like enzyme-linked immunosorbent assay kit [12], [13] or electrochemical sensors [14], [15] are also labor-intensive due to chemical operations and destructive to sashimi, which cannot achieve automatic and passive monitoring. Some recent works [16]–[18] try to achieve cost-effective and automatic daily food monitoring by using spectral reconstruction (SR) techniques, making low-cost spectral cameras possible to achieve similar sensing performance as laboratory-grade HSI cameras.

However, because of the low concentration of histamine levels in the sashimi samples, its spectral characteristics are easily overwhelmed by other ingredients such as protein, whose spectral information is irrelative and redundant to histamine. Thus, it’s essential to conduct feature selection on the HSI data to extract the most useful features that related to histamine prediction. Unfortunately, previous solutions [16]–[18] tend

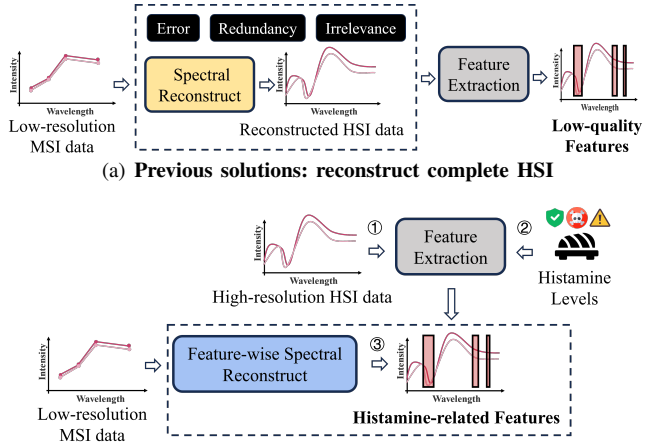


Fig. 2. Comparison of existing spectral reconstruction solution and our feature-wise reconstruction solution.

to reconstruct complete hyperspectral data without filtering out redundant or irrelevant information and even inevitably introduce reconstruction errors during the reconstruction phase (as shown in Figure 2(a)). From such low-quality reconstructed data, it's hard to acquire effective features for histamine prediction.

To narrow this gap, we try to filter out redundant and irrelevant information during the spectral reconstruction process. Figure 2 compares the process of previous spectral reconstruction solutions and our solution. We can apply feature extraction on target HSI before SR and retain only histamine-related features for reconstruction, avoiding reconstructing redundant and irrelevant information. By doing so, we can significantly enhance the correlation between the reconstructed data and histamine values, thereby improving its effectiveness for histamine prediction. However, given the subtle spectral features of histamine, this requires fine-grained feature extraction capability, which cannot be adequately addressed by traditional feature selection methods [19], such as principal component analysis. Inspired by the success of foundation models across various fields [20]–[23], which demonstrate their capability for in-depth feature extraction, we see an opportunity to introduce a spectral foundation model (SFM) into the SR process to obtain more informative features.

Nevertheless, to transform this idea into a practical system, we still face several challenges:

- **Challenge 1: Extract Informative Histamine-Related Spectral Features.** Although previous SFMs [23]–[25] achieves great performance in remote sensing applications, it is trained with remote sensing images, such as trees and fields, whose spectral characters evidently differ from sashimi's and are not related to histamine. When we directly introduce the SFM's encoder in spectral reconstruction, it's hard to extract informative histamine-related spectral features, leading to poor reconstruction performance and bad

histamine prediction results.

- **Challenge 2: Generalization Gap to New Samples.** Due to the differences in colonies and enzymes inside individual sashimi, there may exist large spectral feature differences among different sashimi samples. It is difficult for the base regression model to obtain fine prediction results for new samples collected over time.

To address the above challenges, we present FreshSpec, the first passive and low-cost system for accurate histamine monitoring that requires zero human intervention, utilizing only a commercial multispectral imaging (MSI) camera deployed on-site (as shown in Figure 1). Specifically, FreshSpec achieves this through two novel designs. **Firstly**, instead of reconstructing the full HSI that contains irrelevant and redundant data, FreshSpec exploits a novel feature-wise SR framework that focuses solely on critical histamine-related spectral features, thus greatly improving the quality of reconstructed data for further histamine regression. To achieve this, an SFM encoder is introduced into the reconstruction process and trained with a contrastive scheme to enhance its capability for extracting sashimi samples and histamine-related features. **Secondly**, we notice the monotonic accumulation properties of histamine over time and utilize this property to design an unsupervised model improvement scheme. This scheme ensures the model adapt to new samples using only few unlabeled data, and thus can minimize the generalization gap. Specifically, FreshSpec utilizes unsupervised continual learning to make the model continually self-improve to new sashimi samples during practical deployment through constraints on the relationships of pseudo-labels.

We implement the prototype of FreshSpec with a commercial MSI device costing less than \$100, and evaluate its histamine regression performance on 240 sashimi samples covering various sashimi types, including salmons, tunas and snappers, as well as various histamine levels ranging from 0–70 mg/100g. Results show FreshSpec can achieve an average R² value of 0.9319 and RMSE value of 3.101 mg/100g, which is comparable to lab-level HSI performance and greatly outperforms the baseline schemes (reducing 2.744 mg/100g in RMSE and improving 0.1631 in R²). Moreover, FreshSpec is robust to various environmental changes, including capturing locations, heights, illumination, sashimi size and thickness.

In summary, our main contributions are as follows:

- We introduce FreshSpec, the first passive and low-cost MSI-based system designed to accurately monitor the freshness level of sashimi (*i.e.*, histamine) in display showcases.
- We propose a novel feature-wise spectral reconstruction scheme that effectively reconstructs histamine-related spectral features by leveraging a fine-tuned spectral foundation model. Meanwhile, we present an unsupervised model improvement scheme for adapting the regression model to unseen sashimi samples over time.
- We evaluate FreshSpec's performance over 240 samples of salmon, tuna, and snapper. The results demonstrate the effectiveness of FreshSpec with R² of 0.9319 and RMSE of 3.101 mg/100g, greatly outperforming baseline schemes with a 46.95% RMSE reduction and a 0.1631 R² improvement.

- Our datasets, which include a reconstruction dataset comprising 712 paired MSI-HSI images and a regression dataset containing 1,440 MSI-histamine data groups, will be made openly accessible in [26] upon acceptance of this paper.

The rest of our paper is organized as follows. Section II overviews the related works of histamine detection and HSI. Section III introduces the system designs of FreshSpec including feature-wise spectral reconstruction and regressor's unsupervised continual adaptation. Section IV presents the implementation details and Section V presents the performance evaluation results of FreshSpec. We discuss FreshSpec's limitations and potential extensions in Section VI and conclude our paper in Section VII.

II. RELATED WORK

Before we dive into the details of our design, we review the background and existing works related to fish histamine detection, hyperspectral reconstruction, spectral foundation model, and unsupervised continual learning, in this section.

A. Histamine Detection.

Histamine Management. Histamine is a toxic metabolite produced by certain bacteria during the spoilage and fermentation of fish. Since hazardous histamine levels do not affect the food's taste or appearance, control measures must be implemented throughout the food chain. The most effective method for controlling histamine production is time and temperature management, such as refrigeration and freezing. Without proper temperature control, histamine levels can rise rapidly. For instance, toxic levels of histamine can form in 2 to 3 hours in fish stored at 20 °C or greater [2]. However, in settings like sushi restaurants or fresh food stores, where maintaining refrigeration or freezing conditions is challenging, the freshness and safety of the sashimi samples can not be ensured.

Moreover, as mentioned in FDA guidance document [27], once the fish histamine is formed, it cannot be removed by subsequent activities, such as washing, freezing or heating. Thus, histamine will accumulate monotonically in sashimi over time. Here "monotonic" means that histamine in sashimi will not decrease over time, which is irrelevant to the increase speed. For example, freezing can limit the histamine growth rate but the formed histamine value will not decrease.

Histamine Detection Methods. As shown in Table I, early detection methods primarily used high-performance liquid chromatograph [8], [9], colorimetric assays [28] or mass spectrometry techniques [29], which require expensive laboratory instruments and reagents to obtain reliable results through chemical experiments. The laboratory procedures are time-consuming and costly. More recent technologies have emerged for histamine analysis such as electrochemical biosensors [14], [15], enzyme-linked immunosorbent assay kit [12], [13], fluorescence [30], and hyperspectral imaging [10], [11]. While using electrochemical biosensors like nonenzymatic sensors, assay kits or fluorescence probes is low-cost, these methods still require several chemical operations, limiting their accessibility for average users. They need destructive sampling for each sashimi to conduct chemical experiments, and thus with

TABLE I
COMPARISON OF OUR SOLUTION FRESHSPEC WITH EXISTING HISTAMINE DETECTION TECHNOLOGIES

Method	Cost	Chemical Operations	Accuracy
Chromatography [8]	High	Yes	ng/100g-level
Mass Spectrometry [29]	High	Yes	ng/100g-level
colorimetric Assays [28]	High	Yes	ng/100g-level
Hyperspectral Imaging [10]	High	No	mg/100g-level
Electrochemical Sensor [14]	Low	Yes	ug/100g-level
Fluorescence Sensor [30]	Low	Yes	ug/100g-level
Enzyme-linked Immunosorbent Kits [12]	Low	Yes	mg/100g-level
FreshSpec (ours) (Multispectral Imaging)	Low	No	mg/100g-level

labor-intensive operations. So, these methods cannot automatically monitor the histamine levels. Hyperspectral image (HSI) technology could be the best choice to provide passive and **automatic** histamine monitoring, which doesn't need any of the sample preparation and chemical operations. In theory, HSI can identify -CH bonds generated by decarboxylation during histamine production [31], [32]. However, existing HSI-based histamine monitoring product [32] relies on a complicated and highly expensive hyperspectral camera, *i.e.*, >\$10000, hindering the accessibility to average users at the end of the food chain.

In conclusion, currently there is no histamine detection method that is both **low-cost** and **automatic** (without any chemical operations), thus unavailable to achieve on-site monitoring in sushi restaurants or fresh food stores. In this paper, we present FreshSpec to enable this, by utilizing low-cost and non-invasive MSI technology for automatic monitoring. With well-designed feature-wise spectral reconstruction, FreshSpec can achieve good detection performance approaching HSI.

B. Hyperspectral Reconstruction.

Spectral reconstruction (SR) is a promising way to solve the *high cost* problem of HSI. As illustrated in Figure 3, spectral reconstruction algorithms can reconstruct the hyperspectral information from limited spectral measurements, such as MSI images, RGB images [33] which can be obtained by *low-cost* devices. Generally, they fall into two categories: prior-based and data-driven methods. Prior-based methods [34], [35] utilize statistical information from hyperspectral images, such as sparsity, spatial structure similarity, and spectral correlation, to identify plausible solutions. In contrast, data-driven methods [36]–[40] leverage the abstract features found in large-scale MSI and HSI image datasets to achieve more accurate results. The spectral reconstruction technology, in recent years, has been used and shown good performance in daily food monitoring tasks like organic fruit classification [17], nutrients estimation [16], and meat fraud identification [18]. By collecting MSI-HSI pairs of food samples to train a spectral reconstruction model in advance, the inputted MSI images from low-cost devices can be reconstructed to high-cost HSI images during practical usage. Then, the reconstructed HSI images will be employed for food composition prediction, in a similar manner to real HSI. In this way, deploying a low-cost MSI camera during practical usage is enough, which could approach the performance of an HSI camera through SR.

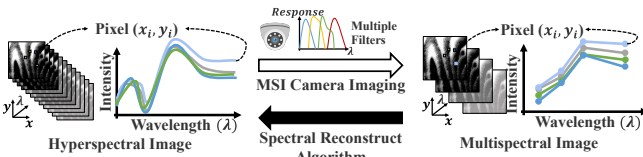


Fig. 3. The process of spectral reconstruction, which can restore the hyperspectral images from limited spectral measurements.

Challenges in Applying SR to histamine prediction.

Despite the great potential of SR, applying it to the task of predicting histamine—a low-concentration trace element—poses critical challenges. All current SR algorithms reconstruct the complete HSI data, while the HSI data contain complex spectral information, some of which are irrelevant to histamine and unhelpful for its prediction. It is crucial to perform feature selection on HSI data to eliminate redundant and irrelevant information. Moreover, the spectral reconstruction process may introduce errors that are randomly distributed across all bands of the reconstructed data. Given that the spectral characteristics of trace elements are subtle, these errors can obscure valuable spectral information of histamine, leading to degraded performance in its prediction. Therefore, this paper proposes reconstructing useful spectral features rather than complete hyperspectral images. FreshSpec employs a spectral foundation model on HSI images to extract fine-grained useful features as the reconstruction target, while filtering redundant and irrelevant information, thereby enhancing the utility of the reconstructed data for histamine prediction.

C. Spectral Foundation Model.

The foundation models are famous at their expertise in effectively capturing complex patterns and representations across various domains [20]–[22]. In the realm of hyperspectral imaging, these models are employed to extract meaningful knowledge representations from intricate spatial-spectral mixed data, addressing challenges in the remote sensing field [23]–[25], [41]. Notably, SpectralGPT [23] achieves superior performance on multiple remote sensing tasks, thanks to its innovative 3D generative pretrained transformer architecture, which is trained on over one million spectral images and boasts over 600 million parameters. SpectralGPT can effectively extract information from spatial-spectral coupling tokens while mitigating hyperspectral redundancy with its attention mechanism and 3D masking strategy. Thus, it's promising to leverage the feature extraction capability of SpectralGPT to assist the spectral reconstruction algorithms.

However, given the training samples are from the remote sensing domain, like trees and fields, whose spectral characteristics and spatial distribution are completely different from that of sashimi samples, SpectralGPT can not be directly used for histamine-related spectral feature extraction. To overcome this challenge, FreshSpec proposes a contrastive-based finetuning scheme for SpectralGPT encoder to capture sashimi histamine-related features.

D. Unsupervised Adaptation and Continual Learning.

In practical applications, for the unseen new sashimi samples with spectral feature differences, the histamine regressor

needs to adapt but there is no prior information about these unseen samples. So, without any labels, the supervised or few-shot domain generalization methods are inapplicable. For the unsupervised adaptation methods for hyperspectral images, such as maximum mean discrepancy (MMD) for distribution alignment [42], [43], adversarial training [44], [45], or self-training [46], all need sufficient data in the target domain, otherwise the distribution of the target domain cannot be learned. However, in our scenario, as the histamine growth (*i.e.*, spoilage) of one sample is irreversible, when we predict its histamine level, we only have the unlabeled data with fewer histamine levels from former timestamps, which cannot measure the overall distribution of target domain. Besides, different from aligning category boundaries in classification, histamine prediction is a regression task where the metrics in the feature space should strictly align with the continuity of labels. Using target sample's limited unlabeled data with an incomplete histamine range cannot achieve this. Thus, these unsupervised adaptation methods cannot apply to our scenario.

As mentioned, the target sample's data quantity is limited and its histamine range is incomplete at only one timestamp. So, the model should be constantly adapted with the updated data distribution to promote its performance. Accordingly, we consider to use unsupervised continual learning (UCL). Existing UCL algorithms employ various self-supervised learning techniques to extract generalized representations of old and new data, such as pseudo-labeling [47] and contrastive loss [48]. Some UCL tasks specifically target representation forgetting [49] or output bias [50]. While these general methods demonstrate a certain usability in tasks like image classification, they are not well-suited for regression tasks like histamine monitoring. In contrast, FreshSpec proposes a novel unsupervised continual learning framework based on the incremental characteristics of histamine.

E. Motivation and Our Objectives

To summarize, FreshSpec aims to achieve low-cost and automatic histamine monitoring, which existing technologies cannot support. FreshSpec attempts to use low-cost MSI and leverage spectral reconstruction to promote its performance approaching HSI. Considering the redundancy and irrelevance problem in existing spectral reconstruction algorithms overwhelming histamine characteristics, FreshSpec proposes reconstructing only useful spectral features instead of complete HSI, where SFM is applied for feature extraction on HSI. Then, to overcome the challenges of (1) spectral patterns gaps in SFM between remote sensing objects and sashimi histamine and (2) spectral feature differences of unseen sashimi samples in practical applications, FreshSpec presents two corresponding designs, with details elaborated in the next section.

III. SYSTEM DESIGN

In this section, we will introduce the detailed design of FreshSpec. Figure 4 shows the overall pipeline of FreshSpec, which consists of three main parts. First, we extract the ROI (*i.e.*, the sashimi area) of collected MSI and HSI images and pair them spatially, in § III-A. Then, we input the preprocessed

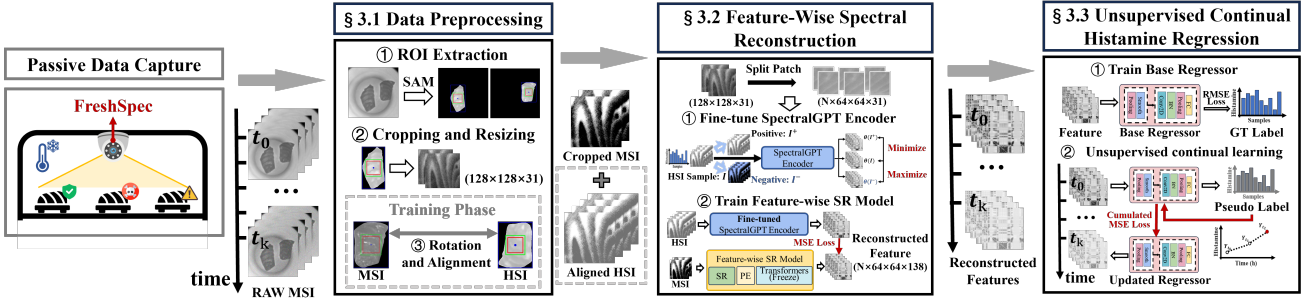


Fig. 4. The system structure of FreshSpec, consists of three parts: data preprocessing, feature-wise spectral reconstruction, and histamine regression with unsupervised continual adaptation.

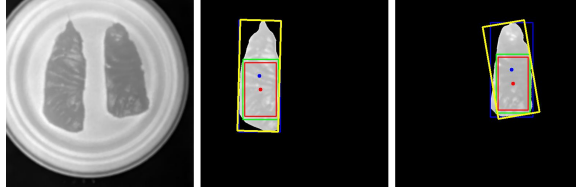


Fig. 5. ROI extraction. The yellow rectangle indicates the minimum enclosing rectangle of the sashimi area after using SAM. The blue rectangle indicates the area after rotation. The green one is the found inscribed rectangle and the red one inside is the final area to extract.

images to train the feature-wise reconstruction (FSR) model, and obtain the histamine-related spectral features during inference phase, as presented in § III-B. Next, for training phase, we input the features to train a base CNN regressor. For inference phase of new sashimi samples, we update the base regressor at each time point, using the proposed unsupervised continual adaptation (UCA) algorithm on new MSI images over time, as described in § III-C. Finally, the histamine prediction results can be derived at each time point.

A. Data Preprocessing and ROI Extraction

A large amount of paired MSI and HSI data is required to train the spectral reconstruction model. The paired data means pixel-to-pixel alignment of the data from two devices, which is impractical to collect physically due to the diversity of hardware parameters and capturing setup. Previous works utilize down sampling to generate large-scale data, which is proven to cause huge performance degradation to real test datasets [17], [18]. To solve this problem, we propose a sashimi sample preprocessing pipeline to extract the sashimi sample area while aligning the MSI image to the corresponding HSI image.

As shown in Figure 5, the pipeline begins with **Ambient Light Elimination**. We conduct background subtraction on MSI and HSI images respectively, by removing the spectral image illuminated solely by ambient light. The collected HSI images have been black-white calibrated in advance by closing the lens cap (black reference) and using the uniform diffuse whiteboard (white reference) [51], which is the camera's built-in function. Next is **Region of Interest (ROI) Extraction**. We employ the Segment Anything Model (SAM [52]) to accurately extract the ROI, based on the clear contrast between sashimi and background. This process generates a binary mask to highlight the selected area. Then, we conduct outlier filtering to refine the masked region by removing the small possible

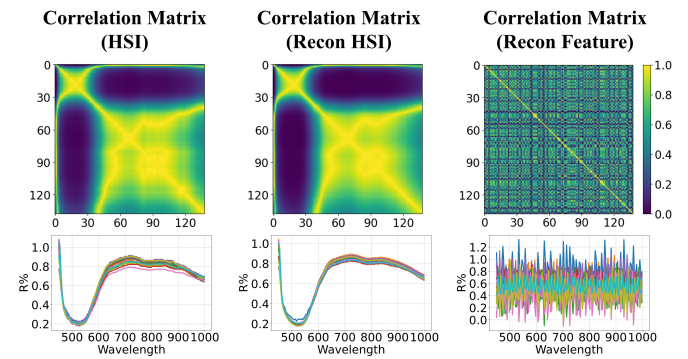


Fig. 6. The correlation matrix of various wavelength bands in raw HSI images, reconstructed HSI images from the SOTA reconstruction model and reconstructed features from FreshSpec.

noise area, ensuring that only the sashimi region is retained. The subsequent phase, **Rotation and Alignment**, involves calculating the smallest enclosing rectangle and adjusting the orientation of both images to 0 degrees. That is, let the contour's bounding box and minimum circumscribed matrix completely overlap. Accordingly, even if the two images are shot at different angles, we can align them to the same angle. Following this, we perform **Cropping and Resizing**, where we identify the maximum inscribed rectangle to crop the image, extracting the relevant ROI from the original image. Then, to avoid the possible shadows during shooting, we take 90% of the internal area after cropping as our final area to extract. Finally, we adjust the dimensions of the cropped MSI and HSI regions to meet the necessary size requirements for further analysis. Based on the above procedure, we can ensure the processed MSI and HSI images are well paired regardless of the two cameras' shooting locations, angles or resolutions.

B. Feature-Wise Spectral Reconstruction

The redundancy of hyperspectral images has been validated in previous works [19], [53]. From the spectral wise, the redundancy refers to both the high correlation between various wavelength bands and involving of irrelevant bands for histamine detection. The correlation matrix in Figure 6 indicates a high correlation in some neighbor wavelengths, which may be useless for subsequent histamine detection. However, these high-correlated information are maintained in the reconstructed spectra from the state-of-the-art (SOTA) spectral reconstruction (SR) model, e.g., MST++ [40]. Furthermore, since the concentration of histamine in the sashimi

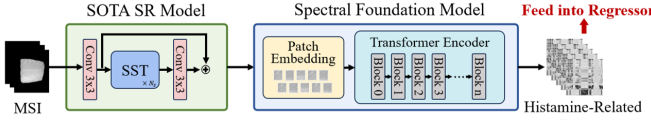


Fig. 7. The architecture of feature-wise spectral reconstruction algorithm.

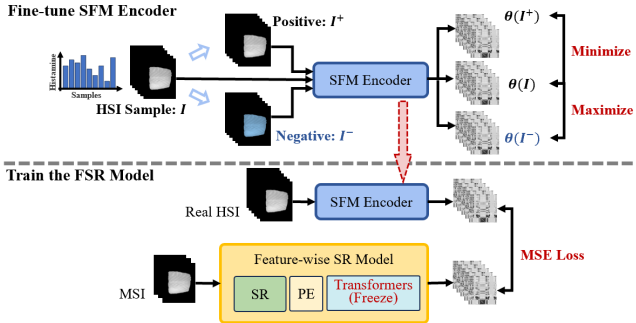


Fig. 8. The training scheme of feature-wise spectral reconstruction algorithm.

sample is pretty low (*i.e.*, the order of magnitude is $mg/100g$), its spectral absorption characteristic is easily overwhelmed by absorption bands of other substances, such as proteins. Moreover, the reconstruction error is consistently spread across various frequency bands of the reconstructed data. This uniform distribution of error in non-essential bands complicates the extraction of valuable information from the reconstructed dataset.

We attempt to solve the above problem by proposing feature-wise spectral reconstruction (FSR). As shown in Figure 7, different from previous spectral reconstruction algorithms, our FSR model targets on reconstructing the most informative spectral feature instead of the full HSI data, which then feeds into the histamine regression model. To reduce the redundancy and extract useful spectral features, we observe that nowadays the large spectral foundation model, *i.e.*, SpectralGPT [23] offers significantly strong capabilities for fine-grained spectral feature representation. SpectralGPT is trained with one million spectral images and contains over 600 million parameters. Its encoder, with deep 11-layer transformers and feature sharing mechanism, can effectively learn the representations from spatial-spectral mixed tokens. Besides, its attention mechanism can capture cross-band spectral dependencies and dynamically assign weights to diminish attention to redundant bands, thus reducing the redundancy of output features. Thus, we can redirect the output of the MST++ spectral reconstruction model into the encoder of SpectralGPT. By applying SpectralGPT’s encoder to the target HSI, we can achieve FSR.

However, the challenge here is that, although SpectralGPT excels in spectral feature representation, it is trained on remote sensing images, which possess spectral characteristics that differ significantly from those of sashimi and are unrelated to histamine. Consequently, directly applying SpectralGPT’s original encoder for spectral reconstruction is likely to result in subpar performance, as the reconstructed features will not correspond to sashimi’s histamine levels, leading to inaccurate predictions.

To this end, we consider to leverage the histamine-related

TABLE II

- (1) RELEVANCE (MI) BETWEEN RECONSTRUCTED DATA AND HISTAMINE.
(2) REDUNDANCY OF RECONSTRUCTED DATA ACROSS CHANNELS.

Solution	Relevance	Redundancy
SOTA SR	0.2989	0.6937
FSR (not fine-tuned)	0.1384	0.3799
FSR (fine-tuned)	0.8153	0.4455

spectral features of our sashimi samples to fine-tune SpectralGPT’s encoder. Specifically, we propose a contrastive-based training scheme to capture spectral features in a soft manner while preventing overfitting. We seek to enhance the feature distance between samples with significant histamine differences while reducing the distance between samples with similar histamine values. Subsequently, we apply the frozen fine-tuned SpectralGPT encoder for histamine-related spectral feature extraction in FSR, as shown in Figure 8.

Fine-tune the Spectral Foundation Model. To ensure the SpectralGPT’s encoder can extract histamine-related embedding, we introduce the histamine value of the sample as prior knowledge and combining with the contrastive learning scheme to guide the fine-tuning process. Specifically, as shown in Figure 8, we select positive and negative samples based on the histamine value difference of the samples. Given histamine difference thresholds K_{h_1} and K_{h_2} , the histamine value difference between positive samples and the target sample is less than K_{h_1} , while the histamine value difference between negative samples and the target sample is greater than K_{h_2} . The thresholds are determined according to our targeted lab-grade HSI performance [5], [10]. Then, we input the HSI data ($64 \times 64 \times 138$) into SpectralGPT’s 3D convolutional layer for patch embedding and next its encoder with 11-layer transformers, and obtain the feature (294×768) in the latent space. Next, we can calculate the features’ Euclidean distance of every two samples. Finally, we fine-tune the encoder by narrowing the feature distance between each sample and its positive samples (*i.e.*, histamine gap $< K_{h_1}$) and increasing that between each sample and its negative samples (*i.e.*, histamine gap $> K_{h_2}$). And the target is to minimize the following loss:

$$\mathcal{L}_c = \mathbb{E}_{I, I^-, I^+} [\log \frac{\exp^{\xi(\Theta(I^+), \Theta(I))}}{\exp^{\xi(\Theta(I^+), \Theta(I))} + \exp^{\xi(\Theta(I^-), \Theta(I))}}], \quad (1)$$

where I, I^-, I^+ indicate the HSI sample and its corresponding negative and positive sample. $\Theta(I)$ refers to the extracted features by SpectralGPT’s encoder, and $\xi(x, y)$ means the mean square distance between the two features. By using this contrastive loss to fine-tune the pretrained SpectralGPT encoder, its output features are able to recognize the subtle differences among sashimi histamine levels. That is, rendering close spectral features for samples with similar histamine levels, while divergent ones for those with distinct levels.

Instead of narrowing the feature difference between remote sensing images and sashimi images, our fine-tuning is to leverage the inherent adaptability of the foundation model to reconfigure its latent representation for task-specific objective, *i.e.*, distinguishing sashimi’s various histamine levels. Thus, the fine-tuned encoder could better capture sashimi spectra patterns and extract the most informative spectral characteristics that are related to histamine.

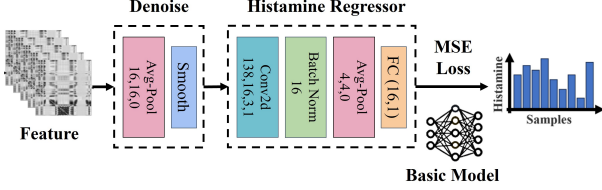


Fig. 9. CNN model for histamine regression.

Train the Feature-wise SR Model. After fine-tuning, we then freeze the transformer structure in the SpectralGPT’s encoder and combine the encoder with SOTA spectral reconstruction model (MST++ [40]). Figure 8 shows the training process of our feature-wise SR model. In this process, the spectral features are extracted using the fine-tuned SpectralGPT’s encoder, which ensures that the model is leveraging its enhanced capabilities to capture important spectral information. To better fit our data condition in terms of resolution and channel number, we do not freeze the patch embedding layer of SpectralGPT before its encoder and let it be jointly trained as a soft constraint. Then we utilize the mean square error between the spectral feature extracted from the real HSI and the spectral feature that output from the feature-wise SR model as loss function, *i.e.*,

$$\mathcal{L}_c = \mathbb{E}_I \|\Theta(I_{hs}) - \Psi(I_{ms})\|^2, \quad (2)$$

where I_{hs} and I_{ms} refer to the HSI and MSI data of the sample I , and $\Psi(\cdot)$ indicate the feature-wise SR model. Therefore, by minimizing the feature gap between real HSI and MSI, the model can not only improve the quality of the reconstructed data but also contribute to a deeper understanding of the spectral characteristics inherent in the data, paving the way for subsequent histamine regression.

Table II measures the histamine relevance and redundancy of the reconstruction results of SOTA SR method, our FSR method and our FSR method without fine-tuning, using salmon samples in our dataset [26]. The relevance is measured with mutual information (MI), a generalized correlation metric for two variables that is sensitive to any kind of functional relationship, not just linear dependencies [54]. We compute MI between reconstructed data and the histamine levels. For the redundancy, we calculate the average value of different wavelength band’s correlation matrix. As we can see, compared to SOTA SR method of reconstructing complete HSI, our FSR method can greatly improve the reconstructed data’s relevance to histamine by $2.73\times$, avoiding reconstructing irrelevant information. If not conducting fine-tuning on SpectralGPT encoder, the relevance would degrade to even lower than SOTA SR, because reconstructing along the original spectral patterns of remote sensing images would deviate more from the sashimi histamine characteristics. This indicates the necessity of fine-tuning and verifies the effectiveness of our approach. Moreover, after fine-tuning, the redundancy slightly increases possibly due to the training manner difference between pretraining and fine-tuning. Despite that, the redundancy of our FSR solution is much lower than SOTA SR by 35.78%, revealing the effectiveness of conducting feature extraction on target HSI for SR.

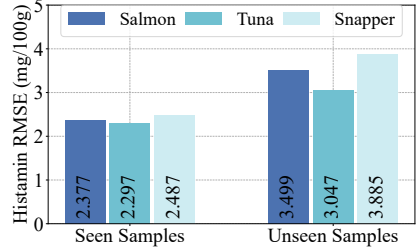


Fig. 10. The generalization gap of the histamine prediction between seen and unseen samples.

C. Histamine Regression and Unsupervised Continual Adaptation

Train the Base CNN Regressor. After feature-wise spectral reconstruction, we consider to train a convolution neural network (CNN) to predict the histamine level from the reconstructed features. To better ensure the integrity of spatial-spectral information, here we choose the reconstructed 3D feature in the latent space as input to our CNN model instead of the 2D feature in the last layer. Before inputting into our CNN model, we conduct a few denoising operations to avoid overfitting. First, we use average pooling and a sliding window for moving averages to reduce the effect of feature noise. Then, we input the cleansed feature ($4 \times 4 \times 138$) which passes through a convolution layer, a batch normalization layer and an average pooling layer in sequence. A 16-length vector could be derived. We exploit it in a fully-connected layer to obtain the histamine prediction result, as illustrated in Figure 9.

Although our proposed CNN-based histamine regression model achieves good performance on seen samples, we observe a performance degradation when applying the model on unseen sashimi samples. As shown in Figure 10, for salmon, tuna and snapper, their root-mean-square-errors on new samples are all significantly higher than seen samples. This stems from the differences in colonies and enzymes inside individual sashimi sample, which may indicate diverse spectral features among different samples. Thus, it’s essential to provide an adaption method to ensure the model’s performance on unseen samples.

Unsupervised Continual Adaptation of Histamine Regressor. To solve this challenge, we propose an unsupervised continual learning method to update the histamine regressor, which can adapt the CNN regression model to new samples without labels. The method is based on two foundations: monotonic accumulation properties of histamine and a huge amount of unlabeled MSI data. Figure 11 illustrates the MSI images of a salmon sample at various timestamps. Specifically, we collect MSI images of the sample at each timestamp I_{t_k} . However, as the histamine label is impossible to obtain in the practical scenario, for a sample at long intervals (*e.g.*, Y_{t_2}) whose histamine label is currently needed to predict, we don’t know the histamine level of this sample in previous timestamps, *i.e.*, t_0 and t_1 . Accordingly, we cannot conduct supervised continual learning for model adaptation. Nevertheless, as the monotonic accumulation properties of histamine, we can ensure that $Y_{t_2} \geq Y_{t_1} \geq Y_{t_0}$. In this way, by limiting the model’s prediction of continuous timestamp for the same sample to follow the incremental property, we are able to

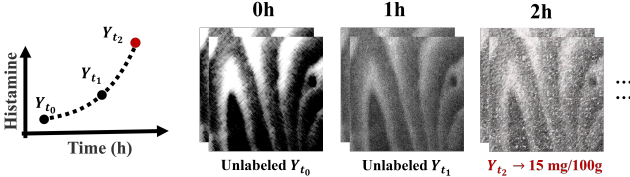


Fig. 11. The monotonic accumulation properties of histamine and corresponding unlabeled MSI images.

achieve unsupervised calibration models on new samples. Specifically, if the pseudo-label predicted from the current timestamp's MSI is less than the pseudo-label from the last timestamp's MSI, which violates the histamine incremental property, we will adapt the model to minimize this error gap to 0. That is,

$$\mathcal{L}_r = \mathbb{E}_I \|\Phi_k(\Psi(I_{t_{i+1}})) - \Phi_k(\Psi(I_{t_i}))\|^2, \\ \text{if } \Phi_k(\Psi(I_{t_{i+1}})) < \Phi_k(\Psi(I_{t_i})) \quad (3)$$

where Φ denotes the current regression model not adapted yet to get pseudo-labels from MSI images. I_{t_i} means the MSI images at i -th timestamp. Eqn 3 leverages only the histamine increment relationship between every two timestamps, *i.e.*, $\Phi_k(\Psi(I_{t_{i+1}}))$ should be greater than $\Phi_k(\Psi(I_{t_i}))$, regardless of the increase speed. That is, as long as $\Phi_k(\Psi(I_{t_{i+1}})) > \Phi_k(\Psi(I_{t_i}))$ holds, the loss function (Eqn 3) will not take it into account during the calculation, no matter what the value $\|\Phi_k(\Psi(I_{t_{i+1}})) - \Phi_k(\Psi(I_{t_i}))\|$ is.

We constantly adapt the model at every timestamp for each sample. For example, for a sample at t_2 timestamp to predict, its model will be firstly updated at t_1 based on the pseudo-labels generated using the basic regression model and secondly updated at t_2 according to the pseudo-labels obtained using the adapted model at t_1 . For t_k timestamp, after acquiring MSI I_{t_k} , we use the updated model at t_{k-1} to generate the pseudo-labels, and judge whether the pseudo-labels of every two adjacent timestamps $(t_0, t_1), (t_1, t_2), \dots, (t_{k-1}, t_k)$ satisfy histamine increment relationship. Those violating the increment relationship will be regarded as error cases. Then, we minimize the sum of these cases' error gaps $\sum_{i=0}^{k-1} \mathcal{L}_r(t_i, t_{i+1})$ to update the regression model to generate more accurate pseudo-labels following histamine accumulation property.

Note that different from the usage of pseudo-labels in past methods to supervise the learning, our pseudo-labels here are variables to optimize instead of labels during the adaptation. Our method's purpose of model adaptation is to make the generated pseudo-labels more accurate which follow the histamine accumulation property and minimize the error cases violating this property, as defined in Eqn 3. The reduction in such error cases could benefit the histamine prediction accuracy. So our method would not incur error accumulation. Instead, with more unlabeled MSI images collected over time, our method can achieve higher calibration performance with more information of target sample's features.

Besides, catastrophic forgetting is inevitable during continual learning, especially in an unsupervised manner. The prediction value may get more and more biased even if it satisfies the histamine incremental property. So, during each iteration in the above model adaptation, we design to re-train

Algorithm 1: Framework of Unsupervised Continual Regressor Adaptation.

Input: Feature-wise SR model: $\Psi(\cdot)$; CNN-based histamine regression model: $\Phi_0(\cdot)$; MSI images of the new sample in continuous timestamps: $I_{t_0}, I_{t_1}, \dots, I_{t_n}$; MSI image set of all seen samples in training dataset: \mathcal{I}_{train} ; Current timestamp: t_k ; Mean square error loss: $\mathcal{L}(\cdot)$.

Output: Histamine value of the last timestamp t_n and update regression model $\Phi_n(\cdot)$.

```

1 Initialize current timestamp and current regression
   model:  $t_k = t_1, \Phi_k(\cdot) = \Phi_0(\cdot)$ 
2 while  $t_k \leq t_n$  do
3   for epoch = 1, 2, ...,  $\delta$  do
4     Obtain pseudo-label of the current timestamp:
5      $Y_{t_k} = \Phi_k(\Psi(I_{t_k}))$ ; Initialize loss:  $\mathcal{L}_{t_k} = 0$ 
6     foreach timestamp  $t_i$  in  $[t_{k-1} \sim t_0]$  do
7       Obtain pseudo-label:  $Y_{t_i} = \Phi_k(\Psi(I_{t_i}))$ ;
8       if  $Y_{t_{i+1}} < Y_{t_i}$  then
9          $\mathcal{L}_{t_k} += \mathcal{L}(Y_{t_{i+1}}, Y_{t_i})$ ;
10      end
11    end
12    Update  $\Phi_k(\cdot)$  by minimizing  $\mathcal{L}_{t_k}$ .
13    Update  $\Phi_k(\cdot)$  by retraining with  $\mathcal{I}_{train}$ .
14  end
15 Calculate  $Y_{t_n} = \Phi_k(\Psi(I_{t_n}))$  and apply  $\Phi_n(\cdot) = \Phi_k(\cdot)$ .

```

this model using the base regression model's training data (seen samples with labels). In this way, we can control the model convergence direction and avoid prediction bias.

The above model adaptation process is individually operated for each sample, for achieving better generalization performance to each sample. This can also avoid the abnormal samples affecting the other samples' prediction. All samples' adaptation starts from the base regression model, respectively. As the size of the regression model is small with only 84KB and one-time adaptation needs 160.58M floating-point operations, separately conducting constant adaptation for each sample brings very little storage cost and computational cost. For example, suppose there are 300 sashimi samples in the showcase, the storage cost of all models is only 24.6MB and the overall computational cost is only 48.2G floating-point operations (while NVIDIA T4 GPU can reach 65 TFLOPS). These are extremely small overheads for the cloud server side. Figure 12 shows the model adaptation results of eight typical samples in our dataset [26], whose ground truth is collected at t_4 . At every timestamp of t_1-t_4 , we update the model and use the updated model for histamine prediction and RMSE calculation. As we can see, our method can work on whether the low-RMSE samples or high-RMSE samples, since it relies on histamine increment relationship instead of absolute error of prediction. And the RMSE exhibits a decreasing trend over time. This is because, with more MSI images collected over time, we can judge more data pairs' increment relationship and adapt to more accurate prediction results.

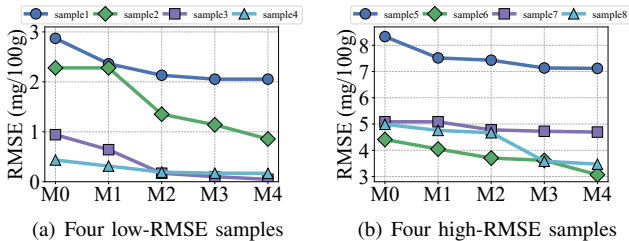


Fig. 12. RMSE changes of sashimi samples with model adaptation of UCA. M0 is the base regression model, and M1-M4 are the adapted models using MSI images collected over t_0-t_4 . Each model is used to predict the histamine value of t_4 's MSI image, and calculate the RMSE with ground truth.

Algorithm 1 depicts the detailed steps of our unsupervised continual regressor adaptation method (UCA), in which we use the size relationship of pseudo-labels over the time series to constantly update the regression model. Our UCA algorithm depends only on the accumulation property of histamine, regardless of irregular increase speeds in different environments.

IV. IMPLEMENTATION

We implement a compact and low-cost prototype using an off-the-shelf multispectral camera [55] and light components. Figure 13(a) illustrates the practical working scenario of FreshSpec, where the system is deployed at the top of the sashimi showcase with a distance to the sample. In our basic setups, the distance is about 20 cm, which is a common height of sashimi showcases. To minimize the system size while avoiding direct leakage of light sources into the camera, we design a two-layer structure of the prototype. As shown in Figure 13(b), the LED array is deployed at the top layer while the multispectral camera is at the bottom layer, within a layer distance of 2cm. Meanwhile, the 7 full-band halogen lamps (VCC7216-ND) are uniformly placed at the top layer to ensure sufficient light intensity and uniform light field. As a result, the size of the prototype is only 9cm × 9cm × 2cm, which is easily deployed into any commercial refrigerators in sashimi restaurants or fresh food stores.

Hardware. We deploy the SEETRUM SEE8820 MSI camera [55] at the center of the bottom layer to capture sashimi MSI images, with a cost of less than \$100. Table III summarizes the basic hardware parameters of our low-cost MSI camera (SEETRUM SEE8820) with comparison of expensive lab-grade HSI camera (Cubert FireflEYE S185). The SEE8820 MSI camera covers both visible and near-infrared bands with wavelengths ranging from 380nm to 980nm. The camera can support no more than 31 various wavelength channels and has a coarse-grained spectral resolution, *i.e.*, 50nm, thereby requiring spectral reconstruction algorithms to enhance. Additionally, the spatial resolution of captured MSI images is 512 × 512, and the frame rate is 30fps, which is promising to provide fast and on-site histamine detection. Among these parameters, the basic requirement of MSI device for histamine prediction, is the wavelength coverage of visible and near-infrared bands. The low spectral resolution of 40-50nm is common in MSI device specifications. And through our spectral reconstruction, we can lead the low-resolution MSI to approach the performance of high-quality HSI, as the results demonstrated in Section V.

Models. Our feature-wise spectral reconstruction model and base histamine regressor are trained using NVIDIA A100 GPU and T4 GPU respectively, and deployed on the cloud server side as well. As the FSR model embeds the SpectralGPT encoder, its computational and memory overhead (see Section V-B3) is probably unaffordable at the edge side. So we conduct all the computation processes on the server side with enough resources. The model training processes are offline completed as follows. The training data of MSI-HSI pairs for reconstruction have been uploaded to the cloud in advance for training the FSR model, which after training is stored and deployed on the server side for practical usage. Similarly, the base regression model is trained with pre-uploaded normal MSI samples with histamine labels on the cloud server. The base regressor is stored and will be used in UCA for new sashimi samples during practical usage.

Practical Usage. During practical usage, the user can set the timestamp interval (*e.g.*, 30 minutes or shorter) to capture the MSI images of sashimi samples monitored in the showcase. The captured MSI images at every timestamp will be automatically uploaded to the cloud server. Then, the server will input the preprocessed MSI into the stored FSR model and output the reconstructed features. Next, for each monitored sample, if it's the first time to upload this sample's MSI image, its reconstructed features will be inputted to the base regressor and output the histamine prediction result. If existing past stored MSI images of this sample, its reconstructed features will be inputted to UCA module to update the current regressor and output the histamine prediction result after fast adaptation. Every time when new MSI images are uploaded, the server will store them separately. Finally, the server will send the predicted histamine levels at this timestamp to the local user. The whole procedure is with little latency (<1 second per sample under 20 Mbps network speed).

V. PERFORMANCE EVALUATION

A. Experiment Setup

1) *Datasets:* We collect an MSI-HSI reconstruction dataset and an MSI-histamine regression dataset, which will be made publicly accessible in [26].

In the MSI-HSI reconstruction dataset, the HSI images with 138 channels and 1024×1024 pixels are collected by Cubert FireflEYE S185 camera and the MSI images with 31 channels and 512×512 pixels are collected by the above Seetrum SEE8820 camera. We put the salmons, tunas and snappers for five hours in lab environment with histamine accumulation and totally 712 pairs of MSI-HSI samples are collected.

In the MSI-histamine regression dataset, the MSI images are collected by the same type of MSI camera deployed on the top of the showcase. The quantity of salmons, tunas and snappers samples is equally 80. We divide them into 5 groups corresponding to time points of 5 hours for images and ground truth collection. The ground truth is obtained by destructive sampling into a standard histamine rapid tester (see Figure 14), with <0.05mg/100g error. For conducting continual learning, each group's samples will be collected MSI at their former

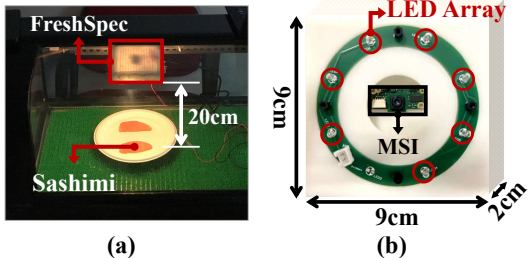


Fig. 13. Practical working scenario and prototype of FreshSpec.

TABLE III

HARDWARE PARAMETERS COMPARISON OF TWO DEVICES: SEETRUM SEE8820 (MSI) AND CUBERT FIREFLEYE S185 (HSI)

Parameters	Seetrum (MSI)	Cubert (HSI)
Channel Range	380~980nm	450~1000nm
Channel Number	31	138
Spectral Resolution	50nm	8nm
Spatial Resolution	512×512 pixels	1000×1000 pixels
Cost	≈ \$100	>\$10,000

time points. That is, we collect 80 samples' data at the first time point and 64 samples' data at the second one. For each sample, we capture two MSI images every time. Accordingly, we get 1440 MSI images in total on 240 salmon, tuna and snapper samples for histamine regression.

The fish species- salmon and tuna used in our dataset are the most common sashimi types globally [56], [57]. For example, salmon accounts for half of the sashimi sold in South Korea [58]. And we use samples from two brands for each sashimi type. Our collected sashimi samples' histamine range from 0 to 70 mg/100g, covering the main freshness interval of 0-40 mg/100g, which is similar to existing histamine detection works [5], [10] and could represent the histamine levels difference. The extremely spoiled samples with >70 mg/100g histamine levels are not much value to predict.

2) *Training scheme*: During the reconstruction period, both MSI and HSI images after alignment are split into patches with 64×64 pixels with a stride of 32. To fine-tune the SpectralGPT's encoder, we set the thresholds of positive-negative samples $K_{h1} = 2$ and $K_{h2} = 4$ according to the lab-grade HSI performance [5], [10], with a batch size of 32 and learning rate of 10^{-4} , and train the encoder for 10000 iterations. Then, for feature-wise spectral reconstruction, we set the learning rate to 5×10^{-4} with cosine annealing to 10^{-6} . The reconstruction model is trained for 50000 iterations in total. For the regression model, we first down-sample the MSI images to 64×64 pixels with nearest neighbor interpolation and conduct average pooling to further reduce the image size to 4×4 . Then, we utilize a batch size of 16 and an initial learning rate of 10^{-4} with cosine decline to 10^{-6} on the Adam optimizer, and train the model for 3000 epochs for convergence. Ultimately, we save this regression model as our basic regression model for the subsequent continual learning part. For every time point, we conduct model adaptation on each sample for 8 epochs with 10^{-6} learning rate via past MSI image. Then, we update our basic model with this new model for the samples on latter time points.

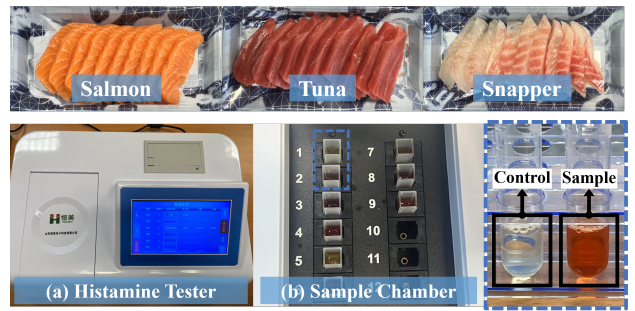


Fig. 14. Sashimi samples and histamine ground truth collection.

3) *Baselines*: Since there is no low-cost automatic histamine detection solution, we consider to apply the SOTA fish histamine prediction methods of high-cost HSI solutions [10], [31], [59], [60] to the reconstructed HSI (reconstructed with SOTA SR model MST++ [40] on MSI) as baselines instead, similar to the works of other foods [17], [18]. Besides, we also take the performance of MSI without spectral reconstruction as a baseline. The details are as follows:

(i) MSI. We input the averaged spectra of MSI images into a partial least squares (PLS) regressor, which is widely used in spectra-based freshness detection area [61].

(ii) MSI (SR) + PLS [10]. As mentioned, similar to [17], [18], we first reconstruct the MSI image with SOTA model MST++ [40] and obtain the reconstructed HSI, denoted as MSI (SR). Then, we conduct principal component analysis on the reconstructed spectra for feature selection and reduction, and then input it into the PLS regressor following [10].

(iii) MSI (SR) + CNN [59]. As the CNN model [59] is for histamine classification task instead of regression, we modify the output dimension of its last layer to one to apply it. Similarly, after getting the reconstructed HSI, we input it into the modified CNN model for training and predicting histamine. Besides, we also employ our CNN model and choose the better performance of the two CNN models as this baseline's result.

(iv) MSI (SR) + WNN [31]. Similarly, after getting the reconstructed HSI, we use the wavelet neural network (WNN) in [31] to train and predict the histamine levels.

(v) MSI (SR) + ViT [60]. Similarly, we modify the last layer and turn the vision transformer (ViT) model for fish freshness classification in [60] to be a regression one. And then we input the reconstructed HSI into it for training and prediction.

Note that FreshSpec's innovation does not lie in the regression model design, but in the feature reconstruction framework. So we compare the FreshSpec with the best performance among the above (ii)-(v) solutions that all use the reconstructed HSI via SOTA reconstruction method MST++ [40]. **We denote the best performance among (ii)-(v) as "MSI (SR)-SOTA".**

4) *Evaluation Metrics*: Since histamine prediction is a regression problem, we exploit the main two metrics for evaluation: R-squared (R2) and root mean square error (RMSE). As mentioned in past works [5], [10], lab-grade HSI (costing >\$10000) can achieve around an RMSE of 2-3 mg/100g and an R-squared of 0.96-0.97. Our MSI-based system (costing only \$100) is targeted to obtain the approaching performance. Besides, according to the FDA regulation of histamine [7], the RSME of a usable solution should not exceed 5 mg/100g.

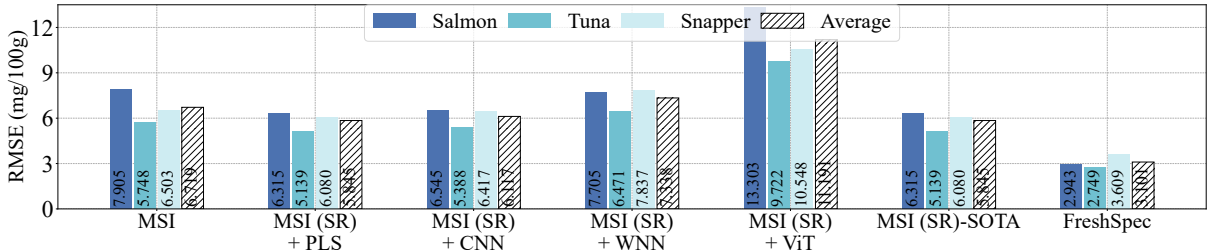


Fig. 15. RMSE comparison between FreshSpec and baselines (i)-(v), where MSI (SR)-SOTA is the best performance using MSI (SR).

TABLE IV
R2 COMPARISON BETWEEN FRESHSPEC AND BASELINES.

Solution	Salmon	Tuna	Snapper	Average
MSI	0.6154	0.6701	0.7385	0.6747
MSI (SR) + PLS	0.7872	0.7595	0.7597	0.7688
MSI (SR) + CNN	0.7672	0.7286	0.7105	0.7354
MSI (SR) + WNN	0.6842	0.6146	0.5766	0.6252
MSI (SR) + ViT	0.0537	0.1731	0.2594	0.1620
MSI (SR)-SOTA	0.7872	0.7595	0.7597	0.7688
FreshSpec	0.9521	0.9252	0.9183	0.9319

B. Overall Performance

We evaluate FreshSpec’s performance with 5-fold cross validation on 80 samples for salmons, tunas and snappers, respectively. The data in the train set and test set are from completely different sashimi samples.

1) *Baseline Comparison*: The overall prediction results are shown in Figure 16 for all three sashimi sample types. It’s obvious that FreshSpec can accurately predict the histamine values for various sashimi types and histamine levels. Figure 15 and Table IV illustrate the RMSE and R2 of the prediction results respectively, revealing important findings. First, FreshSpec achieved significantly better forecast results compared to the baselines. Compared to the current SOTA method, the average R2 of FreshSpec is increased by 0.1631 and the RMSE is decreased by 2.744 where the prediction performance is approaching lab-grade HSI. We can also notice that for the reconstructed data with SOTA SR method, using complex models on them will easily lead to overfitting, due to their redundant and irrelevant information. In contrast, FreshSpec proposes reconstructing only histamine-related useful information to overcome this. Secondly, we note that the solution using SOTA SR has a very limited improvement based on MSI-based solution in histamine prediction tasks comparing with previous tasks [17], only 0.0941. This is because the high redundancy of the HSI data wavelength is very unfavorable to the prediction of histamine, a trace element. In contrast, by using the features-based spectral reconstruction proposed in this paper, the predictive performance of FreshSpec on histamine values has been significantly improved, and R2 has been improved by 0.2572, demonstrating the effectiveness of the system design. Moreover, as we capture two MSI images every time for each sample, their RMSE gaps are only 0.064 on average, indicating the stability of our system. Additionally, three sashimi varieties exhibit slightly different prediction performance, probably due to the diversity of histidine contents and inner chemical components among different sashimi types [62].

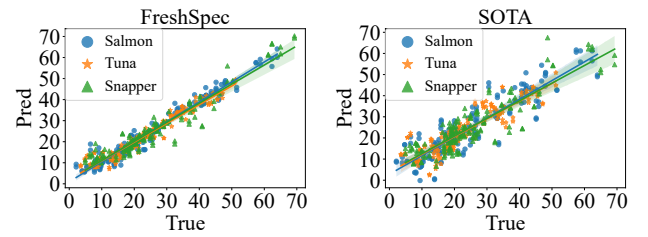


Fig. 16. Histamine prediction results in comparison with the SOTA.

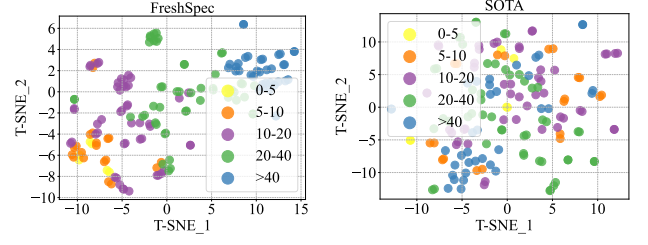


Fig. 17. T-SNE embedding distribution of FreshSpec and the SOTA.

Below we denote the best performance among all baseline schemes as “SOTA”, for comparison with FreshSpec.

2) *Feature-wise Comparison*: To further investigate the effectiveness of FreshSpec’s design, we conduct the two-dimensional t-distributed stochastic neighbor embedding (t-SNE) projections [63] to illustrate the embedding representations of FreshSpec. We classify the samples into five histamine level groups, *i.e.*, 0-5, 5-10, 10-20, 20-40, and >40 mg/100g according to the regulations of different countries on the safe value of histamine [7]. Figure 17 displays the embedding representations of FreshSpec and the embedding of the same salmon samples after the SOTA SR method. We can find that FreshSpec displays much clearer clustering of all five histamine levels than the baseline, indicating its effectiveness in extracting histamine-related information during the reconstruction process.

3) *System overhead and time latency*: Our FSR model with 333.6MB size, has a total parameter number of 87.395M with 30.08G floating-point operations per second (FLOP), due to our usage of large spectral foundation model’s encoder during FSR. Deploying FSR model on the edge imposes significant memory requirements that may exceed the limited resources of edge devices. Therefore, we deploy FSR and conduct all the computations on the cloud server. The inference time for reconstructing one MSI sample’s spectral feature on the NVIDIA T4 Tensor Core GPU is 47.2ms, which can support quick acquisition of spectral features in practical applications.

TABLE V
ABLATION STUDY FOR TWO MODULES FSR AND UCA.

Solution	Salmon		Tuna		Snapper		Average	
	RMSE	R2	RMSE	R2	RMSE	R2	RMSE	R2
SOTA	6.3154	0.7872	5.1395	0.7595	6.0798	0.7597	5.8449	0.7688
MSI (SR) + SFM	5.8861	0.8098	4.8296	0.7894	5.7014	0.7688	5.4724	0.7893
MSI (FSR w/o FT)	6.9442	0.7382	5.8243	0.7065	7.1445	0.6722	6.6377	0.7056
FreshSpec (w/o FSR)	5.3840	0.8409	4.2839	0.8341	5.3215	0.7925	4.9965	0.8225
FreshSpec (w/o UCA)	3.4993	0.9307	3.0471	0.9093	3.8851	0.9053	3.4772	0.9151
FreshSpec (ours)	2.9433	0.9521	2.7494	0.9252	3.6092	0.9183	3.1006	0.9319

Our regression model with 84KB size has a total parameter count of 19.9K and 318.48K FLOP per epoch, and is together deployed on the server side. Only 0.4ms is needed to predict one MSI sample's histamine. Moreover, for the model update in the UCA part, one-time adaptation needs 160.58M floating-point operations for model forward and backward propagation. The measured time latency of adaptation is only 228.3ms for one sashimi sample at every new timestamp, using NVIDIA T4 GPU.

Besides model overhead, we measure the communication overhead of data transfer. Uploading an MSI image with 1.22MB size (compressed by our MSI camera's firmware) needs 611.2ms when the network speed is 20.43Mbps. The latency of returning the histamine result (only several bytes) to the local user could be negligible.

Overall, combining the image capturing latency of 33.3ms per image, reconstruction and regression latency as well as the communication latency, our system can achieve rapid histamine detection with less than 1-second latency for each sashimi sample. Suppose a showcase containing 300 sashimi samples, the overall latency is less than 5 minutes.

C. Ablation Study

We then investigate the modules of FreshSpec by conducting an ablation study to demonstrate the effectiveness of the system design. Table V presents the results of ablation study, where MSI (SR) + SFM denotes the results using features directly extracted by the foundation model after SOTA spectral reconstruction, FreshSpec (w/o FSR) and FreshSpec (w/o UCA) denotes the results only using one module of our system, respectively.

1) *Effectiveness of FSR Module*: Compared to the baseline using the SOTA SR algorithm, the FSR module achieves an improvement of approximately 0.1463 in R2, surpassing the gains of reconstructing HSI from MSI. This result underscores the importance of reconstructing useful features for trace element prediction tasks. Furthermore, it highlights the effectiveness of our proposed FSR module. By employing a contrastive-based fine-tuning method, the large spectral foundation model can extract informative histamine-related features to support subsequent regression tasks. Notably, the improvements from the FSR module are consistent across three types of sashimi samples, demonstrating its general effectiveness. Moreover, directly extracting features of SOTA reconstructed spectra by the foundation model, achieves a limited performance gain of 0.0205 as compared to SOTA scheme. Our method of feature reconstruction can largely

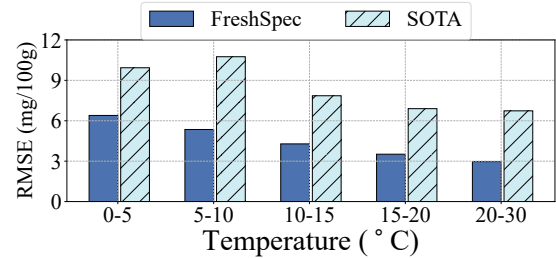


Fig. 18. FreshSpec performance on generalization to various environmental temperatures.

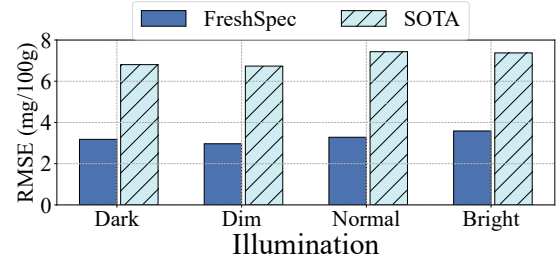


Fig. 19. FreshSpec performance on generalization to various environmental illumination conditions.

promote the R2 by 0.1258, indicating its superiority. Additionally, we can see that, if without fine-tuning the SpectralGPT encoder, the FSR performance would greatly degrade, which is consistent with the feature relevance results in Table II, indicating the necessity of fine-tuning operation in FSR.

2) *Effectiveness of UCA Module*: We designed a CNN-based model to predict histamine values in various sashimi samples and introduced an unsupervised continual learning scheme, *i.e.*, UCA, to enhance its generalization capability for new samples. The effectiveness of the UCA module is reflected in Table V, which shows an R2 improvement of 0.0537 compared to the baseline. While the improvement from the UCA module is modest compared to the FSR module, this aligns with our expectations. The histamine increment relationship between every two timestamps in UCA module is not a strong constraint and needs the underlying model performing relatively well. However, we believe UCA will prove more beneficial in real-world applications, as it can continuously update the model with new, unlabeled data, allowing it to adapt and improve as new samples emerge during deployment.

D. Robustness

Users may use FreshSpec in different scenarios, where environmental brightness, temperature, and even sample properties like size and location may affect the system's performance.

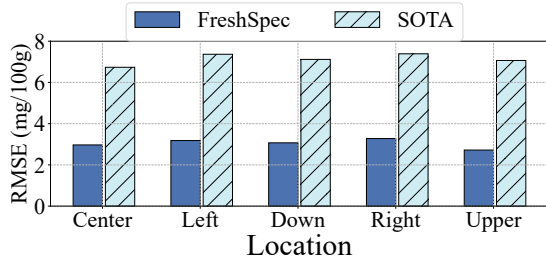


Fig. 20. FreshSpec performance on generalization to various sample locations.

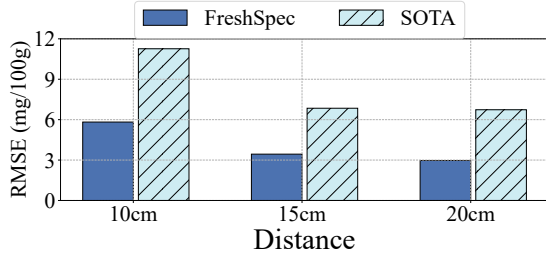


Fig. 21. FreshSpec performance on generalization to various sample-device distance.

Thus we evaluate FreshSpec’s robustness under various experimental and environmental conditions.

1) *Impacts on environmental temperature:* The working scene of the system is in the display cabinet of a sushi restaurant or a fresh food store. Different stores have different temperature settings for display cases, so it is necessary to ensure that the system can work properly at different ambient temperatures. We evaluated the histamine predictions of FreshSpec for 8 salmon samples at ambient temperature levels of 5, and the results are shown in Figure 18. From the figure, we can see that the predicted RMSE of FreshSpec under various ambient temperatures over 5°C is below 5 mg/100g, all of which are better than the best results of the baseline, proving the stability of FreshSpec under various temperatures. This is benefited from our FSR, which can extract features more relevant to histamine, filtering out environmental noises like temperature effects. In addition, we also observed that the prediction performance of FreshSpec became better and better as the ambient temperature rose, which may be due to the temperature drift of the multi-spectral camera used, and the samples of the training set were all collected at normal temperature, with certain deviation. This problem can be solved by calibrating the hardware and is not the focus of this article. Moreover, adding training data under more different temperature setups to enhance FSR, could calibrate it to become more aware of the irrelevant information induced by temperature drift and reconstruct more robust features, which will be explored in our future work.

2) *Impacts on environmental illumination conditions:* Ambient light can interfere with the readings of the MSI camera, which can negatively impact the performance of FreshSpec. Thus, we investigate the performance of FreshSpec under various realistic lighting conditions. We consider four typical light settings: bright (about 550 lx), normal (about 250 lx), dim (about 50 lx), and dark (0 lx). From the results presented in Figure 19, we can observe that, FreshSpec’s performance under different light conditions is very stable. This benefits from

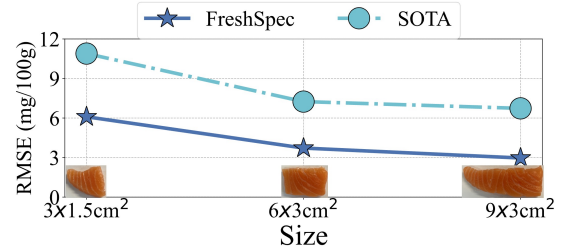


Fig. 22. FreshSpec performance on generalization to various sashimi sample sizes.

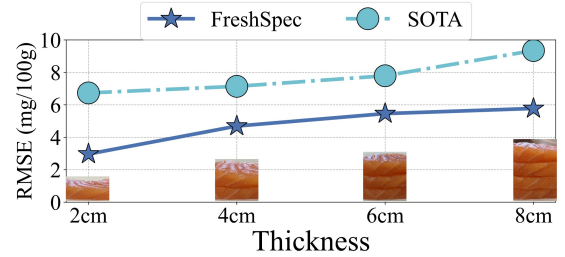


Fig. 23. FreshSpec performance on generalization to various sashimi sample thickness.

the background subtraction steps during the data preprocessing pipeline. Meanwhile, we find that FreshSpec’s performance consistently overwhelms the baseline in all light conditions.

3) *Impacts on sample locations:* As shown in Figure 1, the sashimi samples are not directly put in the central area beneath the camera. In most cases, FreshSpec captures images of the sample with various degrees. Thus, to evaluate the robustness of FreshSpec under various sample locations. We consider the central area and four edge locations, each containing approximately 30° angle with the center of the camera. Figure 20 demonstrates the results, which indicate that FreshSpec is robust to various locations. This is because we utilize a circle-distributed light source that can uniformly illuminate the area. Additionally, by utilizing the cropping step, we only extract the smooth and central area of the sample to conduct analysis, thus avoiding problems caused by uneven light illumination.

4) *Impacts on distance of samples and the device:* As shown in Figure 21, FreshSpec is deployed at the top of the showcases. Considering the different sizes of the sashimi showcases, the distance between the sashimi samples and the camera is varying. Thus, we investigate the performance of FreshSpec by putting the sample at different distances to the camera, including 10 cm, 15 cm, 20 cm. The results are depicted in Figure 21. We can find that the performance of FreshSpec is consistently better than the baseline. However, with the sample getting closer to the camera, the performance of FreshSpec slightly decreases. This is because the focus distance of our selected MSI camera is larger than 20 cm. If the sample is too close to the camera, the captured images are unfocused and contain undesirable noise, which may influence the spectral analysis. Fortunately, the height of sashimi showcases is generally above 15 cm, within the working distance applicable in our multispectral camera.

5) *Impacts on sample size:* The fresh food stores may provide various size of the sashimi samples for selling. Thus, it’s necessary to investigate FreshSpec ’s robustness on various

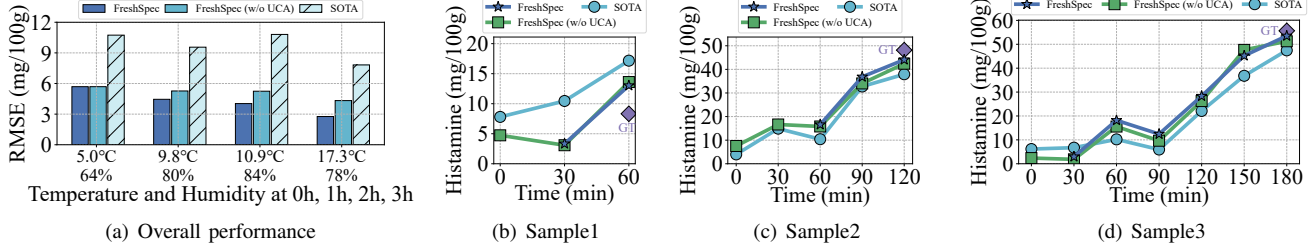


Fig. 24. FreshSpec performance under irregular temperature and humidity changes over time.

sizes of the sashimi samples, especially on small sizes. We select three different sizes of the samples, including $3 \times 1.5\text{cm}^2$, $6 \times 3\text{cm}^2$, and $9 \times 3\text{cm}^2$. Figure 22 shows the results comparing with the baseline. It's obvious that both FreshSpec and the baseline degrade with the sample size decreasing. Since small samples generate small MSI image patches, which contain less spatial information of the data, it's reasonably harder to get an accurate prediction. Nevertheless, we notice that even with a small sample size of $6 \times 3\text{cm}^2$, the RMSE of FreshSpec is still less than 4 mg/100g. And the degradation of FreshSpec is much slighter than the baseline with the sample size squeezing, which indicates better robustness of FreshSpec as compared with the baseline. For the very small size of $3 \times 1.5\text{cm}^2$, we can utilize super-resolution methods to enhance the spatial information, which will be taken into our future work.

6) *Impacts on sample thickness:* The sample thickness of the sashimi thickness may also vary in the stores selling showcases. sashimi samples of different thicknesses may affect the reflection and scattering of light within the sample. For example, a thicker sample would absorb a lot of incoming light, reducing the intensity of the reflected light. Thus, we evaluate the robustness of FreshSpec under various thicknesses of the samples, including 2cm, 4cm, 6cm, and 8cm. Figure 23 illustrates the results, from which we can see that the RMSE of FreshSpec continuously increases with increasing thickness of the sample. This is because the thick sashimi samples absorb more light thus decreasing the collected MSI image quality, making the histamine prediction harder. But we notice the RMSE increasing speed is slowed down once the sample is thick enough, which indicates the lower boundary of FreshSpec's performance. The performance degradation caused by sample thickness can be solved by adding a stronger light source. Currently, we use only 7-LED bulbs, out of the energy reserving consideration, which can be extended to more LEDs in the future.

7) *Impacts on irregular temperature and humidity changes:* In real-world applications, the temperature and humidity in display showcases may fluctuate in an uncontrolled manner over time, due to frequent opening of the cabinet or directly exposing to external air. We replicate such scenarios with irregular temperature and humidity changes over 3 hours, by laying ice in our sashimi showcase and randomly opening the cabinet for random durations in each hour. Table VI displays the temperature and humidity measured every 30 minutes. The temperature and humidity variation speeds are irregular, e.g., slow temperature changes within 60 min to 120 min, rapid changes within 120 min to 180 min. After

TABLE VI
EXPERIMENT SETUP OF FIGURE 24: TEMPERATURE AND HUMIDITY CHANGES OVER TIME

Time	Temperature	Humidity
Init	25.1 °C	47%
0 min	5.0 °C	64%
30 min	6.3 °C	74%
60 min	9.8 °C	80%
90 min	10.6 °C	83%
120 min	10.9 °C	84%
150 min	15.2 °C	80%
180 min	17.3 °C	78%

freezing its temperature to 5°C, we start our evaluation of FreshSpec on 8 salmon samples, which are divided into 4 groups corresponding to 0 hour, 1 hour, 2 hour and 3 hour for ground truth collection (destructive collection, only once). We collect MSI images every 30 minutes for each sample during the monitoring. Figure 24 demonstrates the results. Benefiting from FSR's mechanism of filtering histamine-irrelevant information such as environmental noise, FreshSpec can maintain a fine prediction performance regardless of the changing rates of temperature and humidity, which evidently outperforms the SOTA scheme as well. When the temperature and humidity approach the normal setup as our training samples, the performance would be higher. Besides, our UCA method works well under irregular temperature and humidity variations. This is reasonable because UCA's mechanism relies on only the histamine accumulation property, and independent of the histamine increase speed variations. Under such irregular variations between two timestamps, more error cases of base regressor in UCA could be revealed. This can enhance calibrating the regressor to better focus on the unique spectral characteristics of each sashimi sample.

VI. DISCUSSION AND FUTURE WORKS

In this section, we will discuss the FreshSpec's limitations and potential extensions.

Various Sashimi Types. In this paper, we consider histamine monitoring on three common sashimi types (*i.e.*, salmon, tuna, and snapper). FreshSpec develops separate models for each sashimi type, as their differing compositions may present distinct confounding spectral features for histamine regression. In practical applications, we can classify each sashimi sample based on their visual differences using image identification methods, and then apply the corresponding regression model for accurate histamine prediction. Moreover, for any new sashimi type, our FSR model can be fine-tuned with its extracted histamine-related spectral features via few-shot learning. Then, we can follow the same pipeline to

develop a suitable regression model. Our UCA method will continuously update the regression model for each sashimi sample, working independently of the sashimi types.

Coverage Expansion. The robustness results confirm that for each frame, regardless of the salmon’s position within the camera’s field of view (FOV), FreshSpec consistently performs satisfactorily. If the sample is placed outside the FOV, we can deploy the multispectral imaging camera on a rotating head that can adjust to different angles to cover the entire showcase range and collect a MSI video for further analysis, which will be explored in our future work.

Extension Applications. While FreshSpec is designed for histamine monitoring, its feature-wise spectral reconstruction (FSR) method applies to other spectral reconstruction analysis problems, where redundancy and errors are common in reconstructed spectral data. Compared to existing spectral reconstruction models, FreshSpec’s FSR architecture demonstrates significantly improved performance for the same tasks, enhancing low-cost spectral systems’ ability to detect trace elements which require high-quality spectral data. This allows FreshSpec to extend its use beyond sashimi histamine monitoring to other food products with precise spectral analysis needs for trace elements. For example, detecting meat’s total volatile basic nitrogen (TVB-N) [64] or vegetable’s pesticide residues [65]. The SFM encoder in FSR can be fine-tuned with these trace elements’ feature distribution, thereby enabling FSR to reconstruct relevant spectral features.

VII. CONCLUDING REMARKS

This paper introduces FreshSpec, a low-cost spectral imaging system tailored for precise histamine examination in sashimi, operating autonomously without human intervention. To achieve this, FreshSpec employs a novel feature-wise spectral reconstruction framework that minimizes irrelevant information and redundancy while preserving critical histamine-related spectral features, aided by a spectral foundation model encoder. Additionally, FreshSpec introduces an unsupervised model improvement scheme that leverages the monotonic accumulation properties of histamine over time, allowing the model to continuously adapt and improve with new sashimi samples during practical deployment. Experimental evaluations demonstrate that FreshSpec achieves a high accuracy in histamine monitoring, with an average R₂ value of 0.9319 and RMSE value of 3.101 mg/100g across three types of 240 sashimi samples, significantly outperforming the baseline with a 0.1631 R₂ improvement and a 46.95% RMSE reduction. FreshSpec shows great promise for direct deployment in sashimi stores and fresh food restaurants, ensuring the freshness and safety of food products.

VIII. ACKNOWLEDGMENT

This research is supported in part by RGC under Contract CERG 16206122, 16204523, AoE/E-601/22-R, R6021-20, and Contract R8015.

REFERENCES

- [1] P. Yesudhason, M. Al-Zidjali, A. Al-Zidjali, M. Al-Busaidi, A. Al-Waili, N. Al-Mazrooei, and S. Al-Habsi, “Histamine levels in commercially important fresh and processed fish of oman with reference to international standards,” *Food chemistry*, vol. 140, no. 4, pp. 777–783, 2013.
- [2] C. Feng, S. Teuber, and M. E. Gershwin, “Histamine (scombrotoxic) fish poisoning: a comprehensive review,” *Clinical reviews in allergy & immunology*, vol. 50, pp. 64–69, 2016.
- [3] V. E. Gonzaga, A. G. Lescano, A. A. Huamán, G. Salmón-Mulanovich, and D. L. Blazes, “Histamine levels in fish from markets in lima, perú,” *Journal of Food Protection*, vol. 72, no. 5, pp. 1112–1115, 2009.
- [4] J. Yu, Y. Yue, J. Zhang, Z. Jia, and J. Yang, “Advances in technologies to detect histamine in food: Principles, applications, and prospects,” *Trends in Food Science & Technology*, p. 104385, 2024.
- [5] M. Sánchez-Parras, J. A. F. Pierna, V. Baeten, J. M. Muñoz-Redondo, J. L. Ordóñez-Díaz, and J. M. Moreno-Rojas, “Rapid screening of tuna samples for food safety issues related to histamine content using fourier-transform mid-infrared (ft-mir) and chemometrics,” *Journal of Food Engineering*, vol. 379, p. 112129, 2024.
- [6] S. Pochanagone and R. Rittiron, “Preliminary study on the determination of ppm-level concentration of histamine in tuna fish using a dry extract system for infrared coupled with near-infrared spectroscopy,” *ACS omega*, vol. 4, no. 21, pp. 19164–19171, 2019.
- [7] J. DeBeeR, J. W. Bell, F. Nolte, J. Arcieri, and G. Correa, “Histamine limits by country: A survey and review,” *Journal of Food Protection*, vol. 84, no. 9, pp. 1610–1628, 2021.
- [8] S. Tahmouzi, R. Khaksar, and M. Ghasemlou, “Development and validation of an hplc-fld method for rapid determination of histamine in skipjack tuna fish (katsuwonus pelamis),” *Food Chemistry*, vol. 126, no. 2, pp. 756–761, 2011.
- [9] A. Cicero, F. G. Galluzzo, G. Cammilleri, A. Pulvirenti, G. Giangrossio, A. Macaluso, A. Vella, and V. Ferrantelli, “Development of a rapid and eco-friendly uhplc analytical method for the detection of histamine in fish products,” *International Journal of Environmental Research and Public Health*, vol. 17, no. 20, p. 7453, 2020.
- [10] S. Currò, F. Savini, L. Fasolato, V. Indio, F. Tomasello, G. Rampazzo, E. Zironi, G. Pagliuca, T. Gazzotti, L. Prandini, *et al.*, “Application of near-infrared spectroscopy as at line method for the evaluation of histamine in tuna fish (thunnus albacares),” *Food Control*, p. 110778, 2024.
- [11] S. Ghidini, L. M. Chiesa, S. Panseri, M. O. Varrà, A. Ianieri, D. Pessina, and E. Zanardi, “Histamine control in raw and processed tuna: A rapid tool based on nir spectroscopy,” *Foods*, vol. 10, no. 4, p. 885, 2021.
- [12] S. Köse, N. Kakkıkkaya, S. Koral, B. Tufan, K. C. Buruk, and F. Aydin, “Commercial test kits and the determination of histamine in traditional (ethnic) fish products-evaluation against an eu accepted hplc method,” *Food Chemistry*, vol. 125, no. 4, pp. 1490–1497, 2011.
- [13] P. Rogers and W. Staruszakiewicz, “Histamine test kit comparison,” *Journal of Aquatic Food Product Technology*, vol. 9, no. 2, pp. 5–17, 2000.
- [14] S. Leonardo and M. Campàs, “Electrochemical enzyme sensor arrays for the detection of the biogenic amines histamine, putrescine and cadaverine using magnetic beads as immobilisation supports,” *Microchimica Acta*, vol. 183, pp. 1881–1890, 2016.
- [15] N. Kumar and R. N. Goyal, “Silver nanoparticles decorated graphene nanoribbon modified pyrolytic graphite sensor for determination of histamine,” *Sensors and Actuators B: Chemical*, vol. 268, pp. 383–391, 2018.
- [16] H. Hu, Q. Huang, and Q. Zhang, “Babynutri: a cost-effective baby food macronutrients analyzer based on spectral reconstruction,” *Proceedings of the ACM on Interactive, Mobile, Wearable and Ubiquitous Technologies*, vol. 7, no. 1, pp. 1–30, 2023.
- [17] N. Sharma, M. S. Waseem, S. Mirzaei, and M. Hefeeda, “MobiSpectral: Hyperspectral imaging on mobile devices,” in *Proceedings of the 29th Annual International Conference on Mobile Computing and Networking*, pp. 1–15, 2023.
- [18] H. Hu, Y. Zhu, B. Yang, H. Kang, S. Chen, and Q. Zhang, “MeatSpec: Enabling ubiquitous meat fraud inspection through consumer-level spectral imaging,” in *Proceedings of the 30th Annual International Conference on Mobile Computing and Networking*, pp. 861–874, 2024.
- [19] W. Sun and Q. Du, “Hyperspectral band selection: A review,” *IEEE Geoscience and Remote Sensing Magazine*, vol. 7, no. 2, pp. 118–139, 2019.
- [20] J. Devlin, “Bert: Pre-training of deep bidirectional transformers for language understanding,” *arXiv preprint arXiv:1810.04805*, 2018.

- [21] A. Radford, K. Narasimhan, T. Salimans, I. Sutskever, *et al.*, “Improving language understanding by generative pre-training,” 2018.
- [22] K. He, X. Chen, S. Xie, Y. Li, P. Dollár, and R. Girshick, “Masked autoencoders are scalable vision learners,” in *Proceedings of the IEEE/CVF conference on computer vision and pattern recognition*, pp. 16000–16009, 2022.
- [23] D. Hong, B. Zhang, X. Li, Y. Li, C. Li, J. Yao, N. Yokoya, H. Li, P. Ghamisi, X. Jia, *et al.*, “Spectralgpt: Spectral remote sensing foundation model,” *IEEE Transactions on Pattern Analysis and Machine Intelligence*, 2024.
- [24] X. Li, D. Hong, and J. Chanussot, “S2mae: A spatial-spectral pretraining foundation model for spectral remote sensing data,” in *Proceedings of the IEEE/CVF Conference on Computer Vision and Pattern Recognition*, pp. 24088–24097, 2024.
- [25] Y. Cong, S. Khanna, C. Meng, P. Liu, E. Rozi, Y. He, M. Burke, D. Lobell, and S. Ermon, “Satmae: Pre-training transformers for temporal and multi-spectral satellite imagery,” *Advances in Neural Information Processing Systems*, vol. 35, pp. 197–211, 2022.
- [26] FreshSpec, “Freshspec reconstruction and regression datasets.” https://drive.google.com/drive/folders/1JxaEsZXdsywJbPZDxUM2qCZxRofmjhR3?usp=drive_link, 2024.
- [27] Food and Drug Administration, “Sec. 540.525 scombrotoxin (histamine)-forming fish and fishery products –decomposition and histamine (cpg 7108.24) compliance policy guide: Guidance for fda staff.” <https://www.fda.gov/media/182955/download?attachment>, 2024.
- [28] R. Lv, X. Huang, C. Dai, W. Ye, and X. Tian, “A rapid colorimetric sensing unit for histamine content of mackerel using azo reagent,” *Journal of Food Process Engineering*, vol. 42, no. 5, p. e13099, 2019.
- [29] D. Nei, N. Nakamura, K. Ishihara, M. Kimura, and M. Satomi, “A rapid screening of histamine concentration in fish fillet by direct analysis in real time mass spectrometry (dart-ms),” *Food Control*, vol. 75, pp. 181–186, 2017.
- [30] G. Wu, X. Dou, D. Li, S. Xu, J. Zhang, Z. Ding, and J. Xie, “Recent progress of fluorescence sensors for histamine in foods,” *Biosensors*, vol. 12, no. 3, p. 161, 2022.
- [31] O. Pauline, H.-T. Chang, I.-L. Tsai, C.-H. Lin, S. Chen, and Y.-K. Chuang, “Intelligent assessment of the histamine level in mackerel (*scomber australasicus*) using near-infrared spectroscopy coupled with a hybrid variable selection strategy,” *LWT*, vol. 145, p. 111524, 2021.
- [32] H. Photonics, “Fish inspection.” <https://headwallphotonics.com/application-notes/fish-inspection/>, 2024.
- [33] J. Zhang, R. Su, Q. Fu, W. Ren, F. Heide, and Y. Nie, “A survey on computational spectral reconstruction methods from rgb to hyperspectral imaging,” *Scientific reports*, vol. 12, no. 1, p. 11905, 2022.
- [34] Y. Fu, Y. Zheng, L. Zhang, and H. Huang, “Spectral reflectance recovery from a single rgb image,” *IEEE Transactions on Computational Imaging*, vol. 4, no. 3, pp. 382–394, 2018.
- [35] Y. Li, C. Wang, and J. Zhao, “Locally linear embedded sparse coding for spectral reconstruction from rgb images,” *IEEE Signal Processing Letters*, vol. 25, no. 3, pp. 363–367, 2017.
- [36] A. Alvarez-Gila, J. Van De Weijer, and E. Garrote, “Adversarial networks for spatial context-aware spectral image reconstruction from rgb,” in *Proceedings of the IEEE international conference on computer vision workshops*, pp. 480–490, 2017.
- [37] J. Li, C. Wu, R. Song, Y. Li, and F. Liu, “Adaptive weighted attention network with camera spectral sensitivity prior for spectral reconstruction from rgb images,” in *Proceedings of the IEEE/CVF Conference on Computer Vision and Pattern Recognition Workshops*, pp. 462–463, 2020.
- [38] Z. Shi, C. Chen, Z. Xiong, D. Liu, and F. Wu, “Hscnn+: Advanced cnn-based hyperspectral recovery from rgb images,” in *Proceedings of the IEEE Conference on Computer Vision and Pattern Recognition Workshops*, pp. 939–947, 2018.
- [39] Y. Zhao, L.-M. Po, Q. Yan, W. Liu, and T. Lin, “Hierarchical regression network for spectral reconstruction from rgb images,” in *Proceedings of the IEEE/CVF Conference on Computer Vision and Pattern Recognition Workshops*, pp. 422–423, 2020.
- [40] Y. Cai, J. Lin, Z. Lin, H. Wang, Y. Zhang, H. Pfister, R. Timofte, and L. Van Gool, “Mst++: Multi-stage spectral-wise transformer for efficient spectral reconstruction,” in *Proceedings of the IEEE/CVF Conference on Computer Vision and Pattern Recognition*, pp. 745–755, 2022.
- [41] Y. Xi, W. Jia, J. Zheng, X. Fan, Y. Xie, J. Ren, and X. He, “Drigan: Dual-stream representation learning gan for low-resolution image classification in uav applications,” *IEEE Journal of selected topics in applied earth observations and remote sensing*, vol. 14, pp. 1705–1716, 2020.
- [42] J. Qu, W. Dong, Y. Yang, T. Zhang, Y. Li, and Q. Du, “Cycle-refined multidecision joint alignment network for unsupervised domain adaptive hyperspectral change detection,” *IEEE Transactions on Neural Networks and Learning Systems*, 2024.
- [43] M. Cai, B. Xi, J. Li, S. Feng, Y. Li, Z. Li, and J. Chanussot, “Mind the gap: Multi-level unsupervised domain adaptation for cross-scene hyperspectral image classification,” *IEEE Transactions on Geoscience and Remote Sensing*, 2024.
- [44] C. Yu, M. Xu, Q. Zhang, and X. Lu, “Dual intervention constrained mask-adversary framework for unsupervised domain adaptation of hyperspectral image classification,” *IEEE Geoscience and Remote Sensing Letters*, 2024.
- [45] B. Wang, Y. Xu, Z. Wu, Z. Wei, and J. Chanussot, “Unsupervised domain adaption of hyperspectral images based on paring domain discrimination,” *IEEE Transactions on Geoscience and Remote Sensing*, 2024.
- [46] Y. Xiao, Q. Zhao, S. Lyu, H. Zhao, X. Guan, and W. Feng, “Hybrid training-driven unsupervised domain adaptation network for hyperspectral image classification,” 2025.
- [47] J. He and F. Zhu, “Unsupervised continual learning via pseudo labels,” in *International Workshop on Continual Semi-Supervised Learning*, pp. 15–32, Springer, 2021.
- [48] A. M. N. Taufique, C. S. Jahan, and A. Savakis, “Unsupervised continual learning for gradually varying domains,” in *Proceedings of the IEEE/CVF conference on computer vision and pattern recognition*, pp. 3740–3750, 2022.
- [49] M. Davari, N. Asadi, S. Mudur, R. Aljundi, and E. Belilovsky, “Probing representation forgetting in supervised and unsupervised continual learning,” in *Proceedings of the IEEE/CVF Conference on Computer Vision and Pattern Recognition*, pp. 16712–16721, 2022.
- [50] J. He and F. Zhu, “Out-of-distribution detection in unsupervised continual learning,” in *Proceedings of the IEEE/CVF Conference on Computer Vision and Pattern Recognition*, pp. 3850–3855, 2022.
- [51] G. Polder and G. W. van der Heijden, “Calibration and characterization of spectral imaging systems,” in *Multispectral and Hyperspectral Image Acquisition and Processing*, vol. 4548, pp. 10–17, SPIE, 2001.
- [52] A. Kirillov, E. Mintun, N. Ravi, H. Mao, C. Rolland, L. Gustafson, T. Xiao, S. Whitehead, A. C. Berg, W.-Y. Lo, *et al.*, “Segment anything,” in *Proceedings of the IEEE/CVF International Conference on Computer Vision*, pp. 4015–4026, 2023.
- [53] J. Li, Q. Li, F. Wang, and F. Liu, “Hyperspectral redundancy detection and modeling with local hurst exponent,” *Physica A: Statistical Mechanics and its Applications*, vol. 592, p. 126830, 2022.
- [54] R. Steuer, J. Kurths, C. O. Daub, J. Weise, and J. Selbig, “The mutual information: detecting and evaluating dependencies between variables,” *Bioinformatics*, vol. 18, no. suppl_2, pp. S231–S240, 2002.
- [55] SEETRUM, “Fuhong spectral sensing.” <https://www.seetrum.com/en/products/178.html>, 2022.
- [56] DataIntel, “Sashimi market.” <https://dataintelo.com/report/global-sashimi-market>, 2022.
- [57] M. A. Morgan, L. C. Rabonato, R. F. Milani, L. Miyagusku, and K. D. Quintaes, “As, cd, cr, pb and hg in seafood species used for sashimi and evaluation of dietary exposure,” *Food Control*, vol. 36, no. 1, pp. 24–29, 2014.
- [58] N. S. Counci, “Norway: Bringing salmon sushi to your bento box since the 1980s.” <https://en.seafood.no/news-and-media/news-archive/norway-bringing-salmon-sushi-to-your-bento-box-since-the-1980s>, 2022.
- [59] D. K. Ninh, K. D. Phan, C. T. Vo, M. N. Dang, and N. Le Thanh, “Classification of histamine content in fish using near-infrared spectroscopy and machine learning techniques,” *Information*, vol. 15, no. 9, p. 528, 2024.
- [60] J. P. Rodrigues, O. R. Pacheco, and P. L. Correia, “Seabream freshness classification using vision transformers,” in *Iberoamerican Congress on Pattern Recognition*, pp. 510–525, Springer, 2023.
- [61] I. Parewai, M. As, T. Mine, and M. Koeppen, “Identification and classification of sashimi food using multispectral technology,” in *Proceedings of the 2020 2nd Asia Pacific Information Technology Conference*, pp. 66–72, 2020.
- [62] M. Kanki, T. Yoda, T. Tsukamoto, and E. Baba, “Histidine decarboxylases and their role in accumulation of histamine in tuna and dried saury,” *Applied and Environmental Microbiology*, vol. 73, no. 5, pp. 1467–1473, 2007.
- [63] L. Van der Maaten and G. Hinton, “Visualizing data using t-sne,” *Journal of machine learning research*, vol. 9, no. 11, 2008.
- [64] Y. Zhang, H. Xue, Q. Ma, Y. Li, Q. Zhou, J. Sun, and W. Wang, “Potential of two-dimensional correlation-based dual-band visible/near

- infrared spectroscopy to predict total volatile basic nitrogen content in meat," *Journal of Food Composition and Analysis*, vol. 133, p. 106451, 2024.
- [65] J. Sun, S. Cong, H. Mao, X. Wu, and N. Yang, "Quantitative detection of mixed pesticide residue of lettuce leaves based on hyperspectral technique," *Journal of Food Process Engineering*, vol. 41, no. 2, p. e12654, 2018.